Available online at www.sciencedirect.com
SCIENCE DIRECT®
Journal of Nuclear Materials 343 (2005) 70–80
journal of nuclear materials
www.elsevier.com/locate/jnucmat

Pitting damage by pressure waves in a mercury target

M. Futakawa [a,*], T. Naoe [b], C.C. Tsai [c], H. Kogawa [a], S. Ishikura [a], Y. Ikeda [a], H. Soyama [d], H. Date [e]

[a] *Center for Proton Accelerator Facilities, Japan Atomic Research Institute, Tokai-mura, Ibaraki-ken 319-1195, Japan*
[b] *Ibaraki University, Hitachi-shi, Ibaraki-ken, 316-851, Japan*
[c] *Oak Ridge National Laboratory, Oak Ridge, TN 37831, USA*
[d] *Tohoku University, Sendai-shi, Miyagi-ken, 980-8579, Japan*
[e] *Tohokugakuin University, Tagajyo-shi, Miyagi-ken, 985-8537, Japan*

Abstract

Liquid-mercury target systems for MW-scale pulsed spallation neutron sources are being developed. A proton beam will be injected into the mercury target to induce spallation reactions. The moment the proton beam bombards the target, pressure waves will be generated in the mercury by the thermally shocked heat deposition. Negative pressures will cause the formation of short-lived cavities in the mercury. Those cavities that collapse on the interface between the mercury and the target vessel wall will develop pits in the wall surface. In order to investigate the pitting damage due to large numbers of cycles up to 10 million, the pressure waves were simulated electromagnetically in a Magnetic IMpact Testing Machine (MIMTM). The obtained data were compared with erosion data from classical vibratory horn tests and a bubble dynamic simulation was carried out to investigate the repeated frequency effect. It is demonstrated that the mean depth of erosion is predictable using a homologous line in the steady state with mass loss independent of testing machines. The incubation period is shown to depend on materials, repeated frequency and imposed power or pressure.

1. Introduction

The Japan Atomic Energy Research Institute (JAERI) is carrying out research and development on a Neutron Science Project aiming at exploring basic researches into materials and life sciences, and innovative nuclear technology such as actinide transmutation with the accelerator driven system (ADS) [1]. A MW-scale target can produce a high-intensity neutron beam by the spallation reaction due to accelerated protons impinging on the target material. A liquid-mercury target system for the MW-scale target is being developed taking into account the advantages of self-circulating heat removal and neutron yield. Fig. 1 shows a schematic drawing of the liquid-mercury target structure developed by JAERI. The proton beam with a 1 μs pulse duration is injected into the mercury through the beam window at 25 Hz. The moment the proton beam hits the target vessel, thermal stress waves will be imposed on the beam window and pressure waves will be generated in the mercury by the thermally shocked heat deposition [2]. The pressure waves travel through the mercury

* Corresponding author. Tel.: +81 29 282 5363; fax: +81 29 282 6712.
E-mail address: futakawa@popsvr.tokai.jaeri.go.jp (M. Futakawa).

0022-3115/$ - see front matter © 2005 Elsevier B.V. All rights reserved.
doi:10.1016/j.jnucmat.2004.07.063

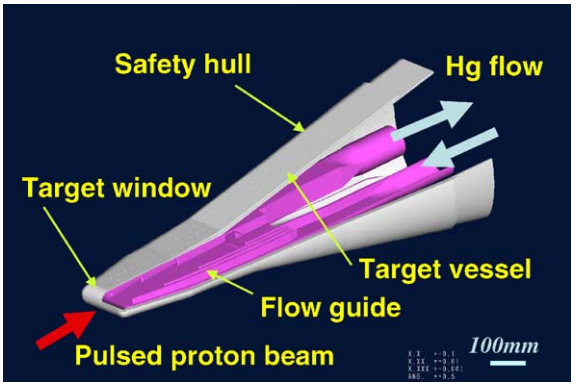

Fig. 1. Schematic drawing of a MW-scale neutron spallation target.

to the target vessel wall and back again. Stress waves are excited by the pressure waves propagating in the vessel wall. The resulting dynamic stress distribution in the vessel wall becomes very complicated. Negative pressure waves can cause cavitation in the mercury, succeeded by collapse of the cavitation bubbles which generates microjets and/or shock waves. Those bubbles that collapse at the vessel wall can form pits on the surface of the wall. This cavitation erosion damage can compromise the structural integrity and reduce the life of the vessel.

In JAERI, plane-strain-wave incident experiments have been carried out using a modified Split Hopkinson Pressure Bar (SHPB), in order to examine the impact response of the liquid mercury and the impact damage at the interface between the liquid mercury and the solid metal specimens [3]. Through a series of tests, the JAERI team found that the solid surfaces in contact with the mercury were eroded by pitting and suggested the possibility of pitting erosion in the target vessel [4,5]. Following the SHPB off-line test, an Oak Ridge National Lab. (ORNL) team carried out the tests at Weapons Neutron Research (WNR) facility in Los Alamos Neutron Science Center (LANSCE) and recognized the pitting damage in the cylindrical target vessel [6]. From the above examinations, the pitting damage is recognized as a new issue to decide the life of the target vessel.

The SHPB test gives quite similar morphology of the pitting to that observed in WNR on-beam test up to hundred impact cycles [7]. However, the imposed number of impacts is limited to approximately 100 at maximum, because the SHPB needs time to adjust for operation. 100 cycles are not enough to extrapolate the lifetime of candidate target structure materials. The proton beams are injected into the target at 25 Hz for Japan Spallation Neutron Source (JSNS) and at 60 Hz for Spallation Neutron Source (SNS). The pitting damage at high cycles over 10 millions should be evaluated to estimate the lifetime of the target. The JAERI team, therefore, has developed a novel device, Magnet IMpact Testing Machine (MIMTM), to electromagnetically impose pulse pressure into the mercury. Data on the pitting damage at high cycle impacts up to 10 million have been obtained in the MIMTM. In this paper, the pitting damage formation, repeated frequency effect, power dependency and estimation of cavitation erosion in the mercury target will be discussed.

2. Experimental

The MIMTM (Max. acc.: ≈300 G) was developed to examine the pitting damage up to over 10 million cycles. The MIMTM consists of the control unit, the magnetic amplifier and the electrically driven pressure pulse actuator. A short cylinder is filled with mercury of approximately 120 cm^3. The pressure pulse is repeatedly imposed at 1 Hz to 200 Hz to the mercury via the circular plate in contact with the mercury, which is driven by the actuator, as shown in Fig. 2. The imposed pressure is precisely and quantitatively controlled by changing the electric current for the magnet coils: i.e. rising time, holding time, sine wave, rectangular wave, repeated frequency, and amplitude of tensile or compressive pressures. In particular, the tensile pressure; negative pressure, is a key condition for the cavitation formation. The imposed acceleration was measured by a piezo-type accelerator and used as a control signal. The pitting damage is affected by the cavitation intensity which is very dependent on the magnitude of negative pressure generated along the interface between the mercury and the wall surface or the specimen surface. In this test, the negative pressure was controlled by the imposed power to the MIMTM precisely to produce the same pit morphology as that observed in the WNR proton beam test.

In the MIMTM, two types of specimens were used. One was a circular plate specimen of diameter 100 mm. The other was a button specimen with a diameter of 15 mm. The highly polished surface of the specimens is in contact with mercury. On the plate specimen,

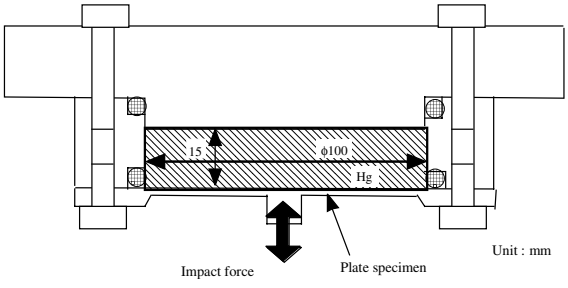

Fig. 2. Mercury chamber in MIMTM.

a sticky tape was used to mask some areas from any pitting damage. The plate specimen was divided into 6 regions and each region was exposed to mercury separately for impact cycle ranges varying up to 10 million, in order to understand formation of the pitting damage for each range of cycles. The button specimen was screwed on the center of the strike plate, whose dimension is the same as the circular plate specimen. The specimens are prepared from 316SS materials (cold worked 20%) with and without surface hardening treatments by carburizing and nitriding. Kolsterising [8], The morphology and 3D-image of pits were examined by a laser microscope (Laser tech. LHD-15H) and scanning electron microscope (SEM, Shimadzu SS330FEG). Mass change of button specimen was precisely measured by a micro-balance (Chyo M1-20A). The eroded area was evaluated digitally using an image analysis program.

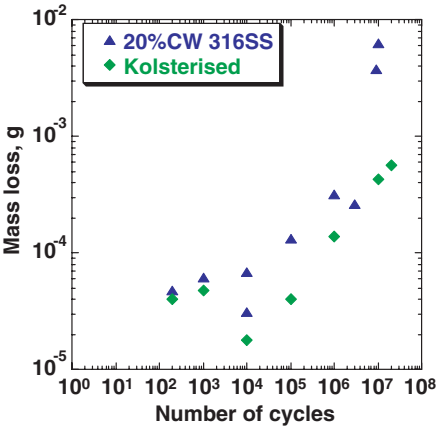

Fig. 3. Dependency of mass loss on number of cycles.

3. Results

3.1. Pitting damage formation

3.1.1. Mass loss

Fig. 3 shows the dependency of mass loss of the button specimens on the number of impact cycles. In the case of 20% CW 316SS, the mass loss increases slightly up to 10^6 impact cycles, and then jumps up at over 10^6 cycles. An acceleration stage occurs between 10^6 and 10^7 cycles. That is, a so-called incubation state prevails at less than 10^6 cycles and a steady state begins at more than 10^6 cycles. The mass loss of the Kolsterised button specimen is much smaller than that of 20% CW 316SS at 10^4 cycles and does not exhibit the acceleration stage even at more than 10^7 cycles.

In order to predict the progress of pitting damage throughout the life of target, the pitting damage for high cycle impacts up to 10^8 cycles at least must be evaluated. In the case of the classical vibratory horn tests, the repeated frequency is approximately 20 kHz generally. The number of cycles gets to be over 10^8 in 1.5 h. Fig. 4 shows the relationship, in mercury, between mean

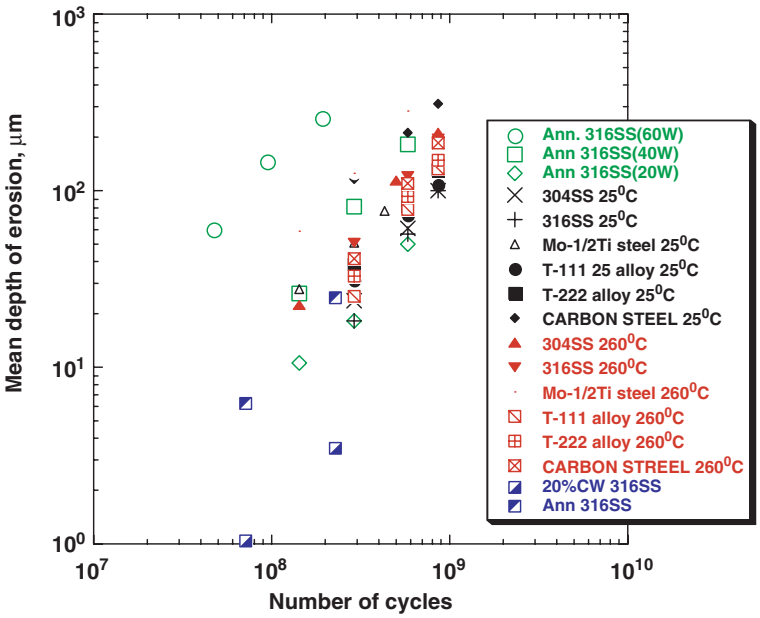

Fig. 4. MDE measured in vibratory horn tests in mercury [9–12].

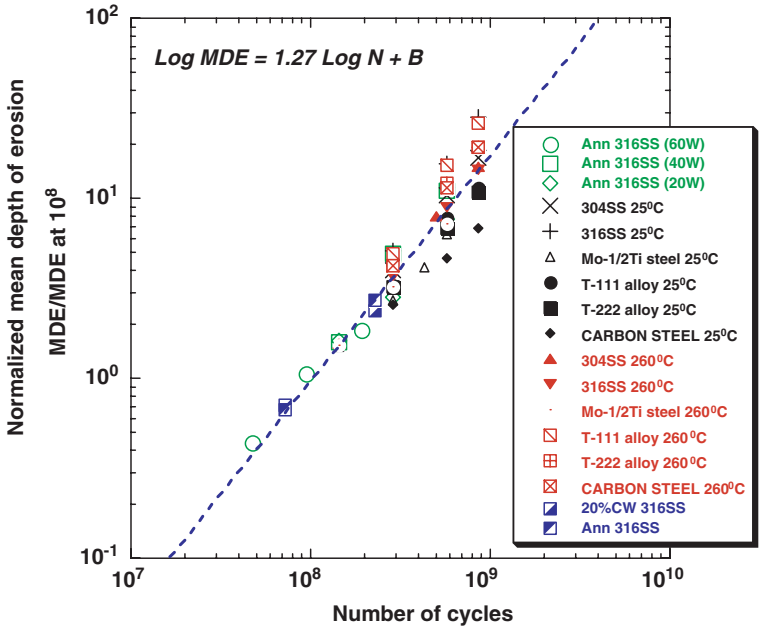

Fig. 5. Normalized MDE data for vibratory horn tests in mercury.

depth of erosion (MDE) and the number of cycles, taken from classical vibratory horn tests carried out in various conditions of temperature, imposed power (watts, W) and materials [9–12]. These data for each material are replotted using the MDE normalized by that at 10^8 cycles, as shown in Fig. 5. It is found that the normalized MDE is adequately plotted on the homologous line given by the equation:

$$\mathrm{Log\,MDE} = A\,\mathrm{Log}N + B, \tag{1}$$

where $A = 1.27$ for mercury, $B = f$ (materials, temperature, power, etc.) and N is the number of cycles. The constant B, which is related to the incubation period, is strongly dependent on the material, and its condition, temperature, and imposed power, while, the A value is independent of materials and cavitation intensity. This tendency has been confirmed in the case of water cavitation erosion as well [13]. That is, the MDE in the steady state is conveniently predictable by using Eq. (1).

The MDE in the MIMTM was evaluated from the data of mass loss shown in Fig. 3, and replotted together in a log-log graph with the results obtained by the WNR proton beam tests with 0.4, 1.2 and 2.5 MW protons [14] and with a vibratory horn for 316SS [9] and Kolsterised 316SS [12], as shown in Fig. 6. In Fig. 6, the line given by Eq. (1) is drawn for 20% CW 316SS in the MIMTM. It is recognized in this case that an incubation period is present up to 10^6 cycles and after that the MDE increases with the number of cycles in compliance with Eq. (1). The incubation period is expanded up to 10^7 cycles by the Kolsterised hardening surface treatment. The inclination of the drawn line describes well the trend of cavitation erosion against number of cycles obtained by vibratory horn, regardless of the imposed power and the surface treatment.

3.1.2. Morphology

Fig. 7 shows the evolution of pitting damage between 10^3 and 10^7 cycles obtained from the circular plate specimens: the laser microscope and 3-D images. The repeated frequency of impact cycle is 20 Hz. The imposed acceleration level is about 980 m/s^2 (560 W) that can reproduce the pit morphology observed in the WNR on-beam tests [7]. The pitting damage is strongly dependent on the number of cycles. It is found that the formation process of the pitting damage is divided into 3 phases. Phase 1 ($<10^4$ cycles): the pitting damage up to 10^4 cycles looks to be occupied by the individual isolated pits. Quite similar morphology of pits was observed in the SHPB and WNR tests. Phase 2 (10^5 to 10^6 cycles): as the number of cycles increases to more than 10^5 cycles, the individual isolated pits appear to combine with each other or overlap and the surface around pits is eroded by peeling out. Phase 3 ($>10^6$ cycles): the pitting damage spreads throughout the surface and homogeneous erosion starts.

The trend of mass loss shown in Fig. 3 is understandable from the viewpoint of microstructure of damaged surfaces. In the case of 20% CW 316SS, the original surface remains up to 10^5 cycles, and over 10^6 impact cycles the original surface disappears and after 10^7 cycles holes larger than 10 μm in diameter are present on the

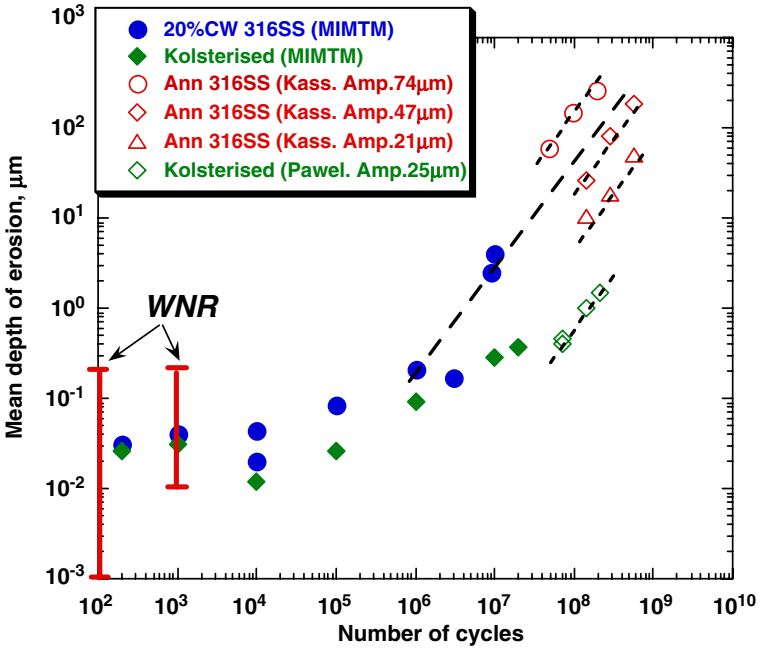

Fig. 6. Relationship between MDE and number of cycles for 316SS.

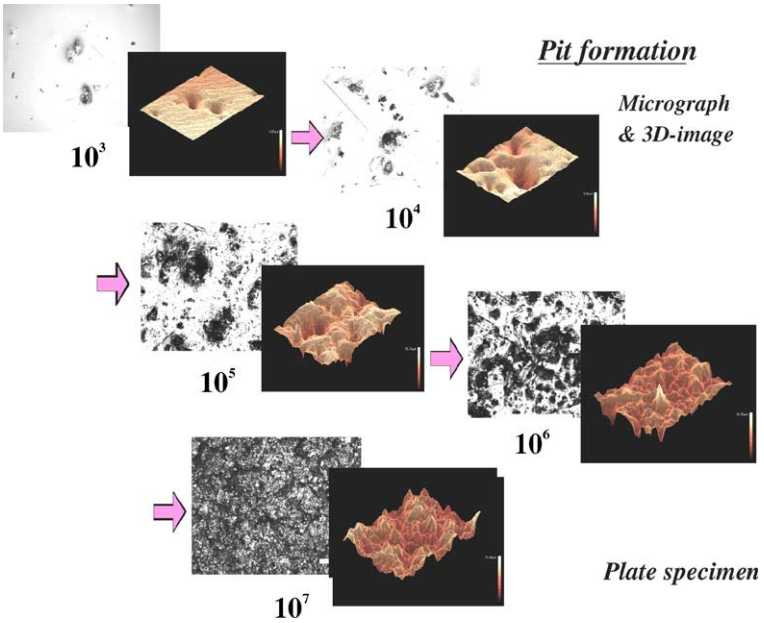

Fig. 7. Pitting damage formation up to 10^7 cycles at 20 Hz.

damaged surface, as shown in Fig. 8. The formation of the holes is associated with the large mass loss.

Fig. 9 shows the comparison of pitting damage morphologies at 10^6 cycles with and without Kolsterising surface hardening treatment. It is unambiguously seen that the damage is reduced dramatically by the Kolsterising hardening surface treatment. In fact, the pitting damage of Kolsterised ones was hardly observed up to 10^5 impact cycles. The Kolsterised specimen exhibits little mass loss up to 2×10^7 cycles. The individual isolated

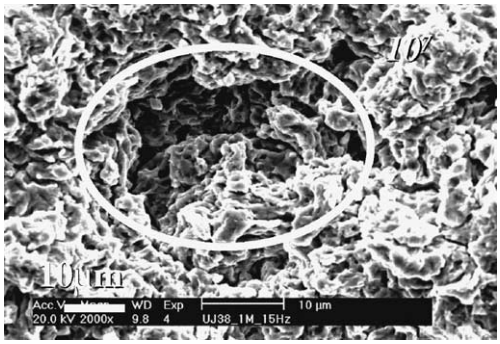

Fig. 8. Hole at 10^7 cycles in 20% CW 316SS.

pits occupy damaged surface in 10^6 impact cycles and overlapped and/or combined pits are observed over 2×10^7 impact cycles, but no holes are recognized unlike 20% CW 316SS.

In order to quantitatively understand the formation behavior of the pitting damage, an image analysis was carried out as illustrated in Fig. 10. The eroded area was defined as the black parts distinguished from the black-white image, and the fraction of the eroded area to the observed area was calculated. The fractions are plotted with the MDEs in Fig. 11. Regardless of materials, the period in which the area fraction less than 1 is equivalent to the incubation period defined earlier from

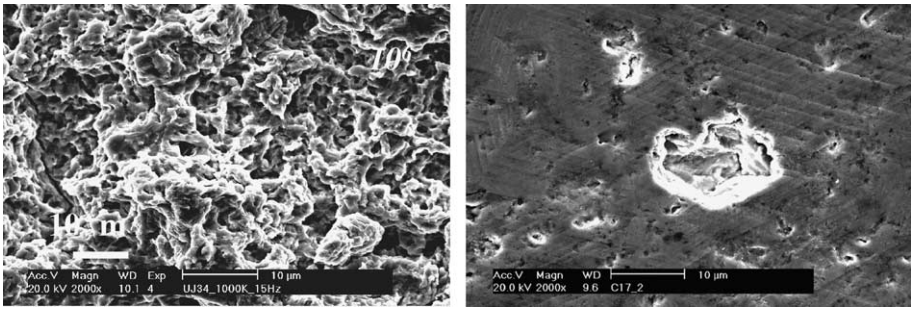

Fig. 9. Comparison between 20% CW 316SS and the Kolsterised condition after one million cycles.

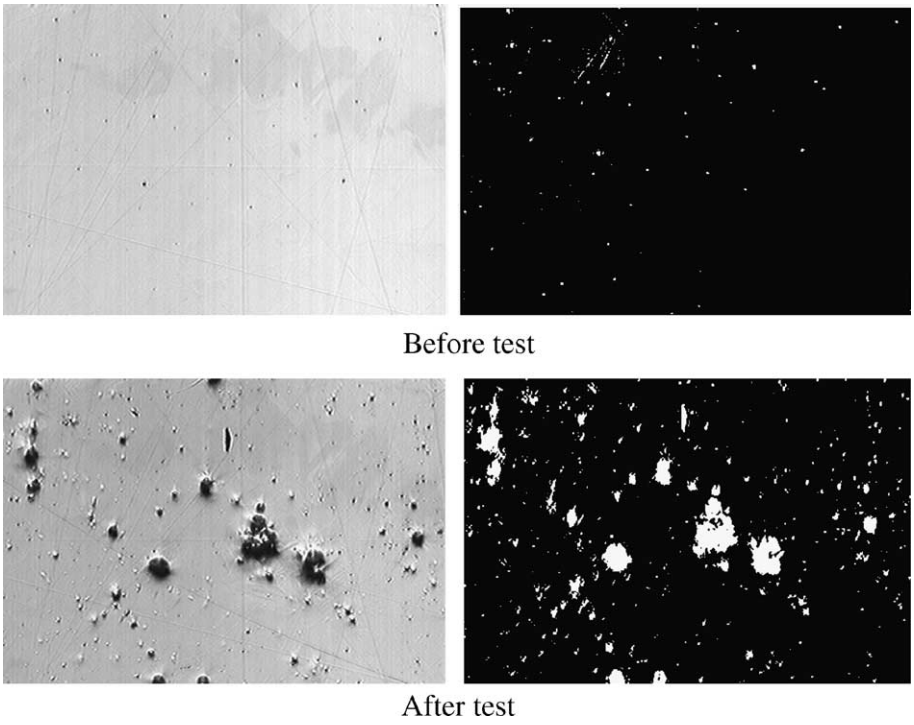

Fig. 10. Pit images transformed from an optical image to a black and white image to facilitate damaged area measurement.

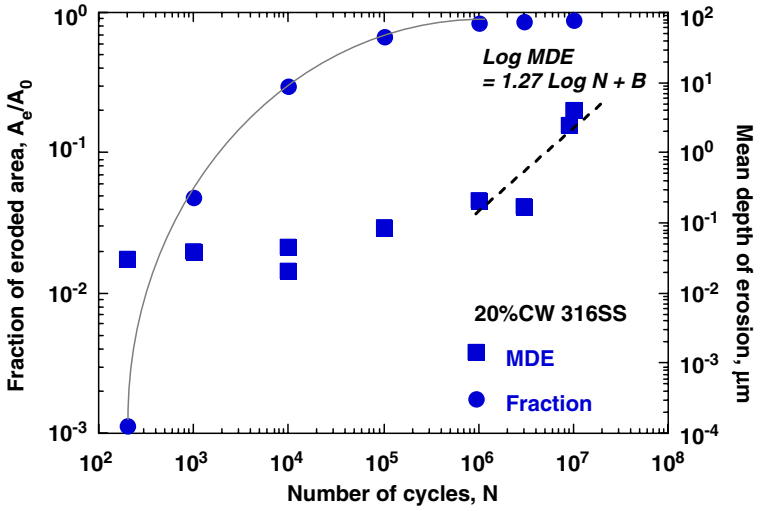

Fig. 11. MDE and fraction in 316SS.

the mass loss data. The locus of fraction appears to increase regularly with the impact cycles.

3.2. Power and frequency effects

Fig. 12 shows the power dependency of dynamic responses measured by the accelerometer fixed at the actuator of MIMTM. The power supplied to the MIMTM was varied from 150 W to 560 W at the repeated frequency of 25 Hz. At 560 W, the high frequency components are superimposed on the vibrational wave with a periodicity of some ms. On the other hand the high frequency components are hardly observed at 260 W. The high frequency components seem to be related to the localized impacts with high energy density due to cavitation bubble collapse. They were extracted through high pass filtering to estimate the cavitation intensity. Fig. 13 shows the typical filtered signal at 560 W and 25 Hz. The damage potential function ϕ was defined as the following equation and calculated from the filtered signals:

$$\phi = \int a_e^2(t)\,dt, \tag{2}$$

$$a_e(t) = \begin{cases} 0 & |a(t)| \leqslant a_{th}, \\ |a(t)|a_{th} & |a(t)| > a_{th}. \end{cases} \tag{3}$$

Here, the threshold a_{th} for no damage was 59 m/s^2. ϕ in Eq. (2) is associated with the accumulated energy for damage by the localized impact. Fig. 14 shows the relationship between the fraction of eroded area at 10^5 cycles, the normalized damage potential ϕ/ϕ_0 and the input power. Here, ϕ_0 is ϕ at 560 W and 25 Hz. Since both the fraction and ϕ/ϕ_0 are almost 0 at power lower than approximately 200 W, it is understandable that the damage threshold appears to be present at above 200 W.

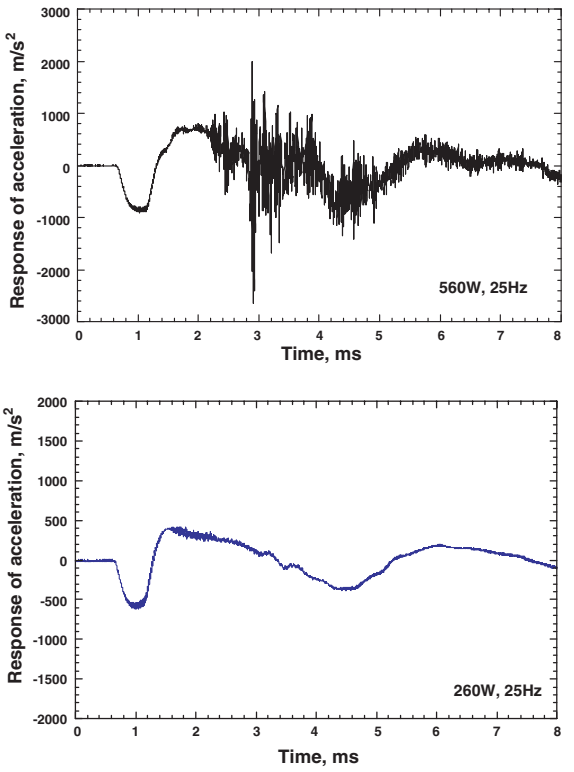

Fig. 12. Measured acceleration at 25 Hz.

Fig. 15 shows the relationship between the fraction of eroded area at 10^5 cycles and 560 W, normalized damage potential ϕ/ϕ_0 and the cycle frequency. The fraction

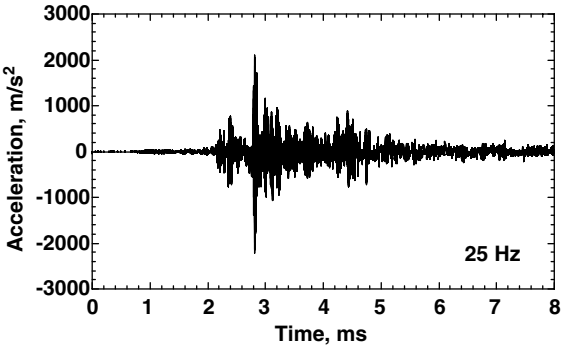

Fig. 13. Filtered acceleration at 25 Hz and 560 W.

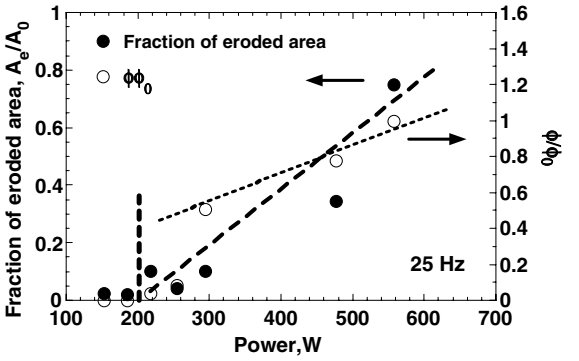

Fig. 14. Relationship between erosion fraction, ϕ/ϕ_0 and power.

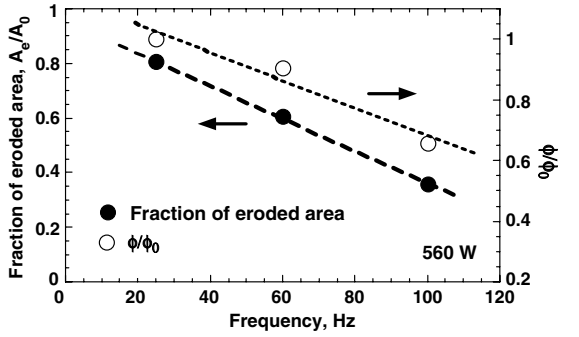

Fig. 15. Relationship between eroded fraction, ϕ/ϕ_0 and frequency.

decreases with the increase in frequency in the experimental frequency range. The fraction exhibits a similar trend of the frequency with ϕ/ϕ_0. Fig. 16 shows the relationship between the fraction and ϕ/ϕ_0. ϕ/ϕ_0 shows the same trend as the damage fraction; damage, for power and frequency. Therefore, it can be said that ϕ/ϕ_0 is a useful parameter to estimate the damage independent of impact condition.

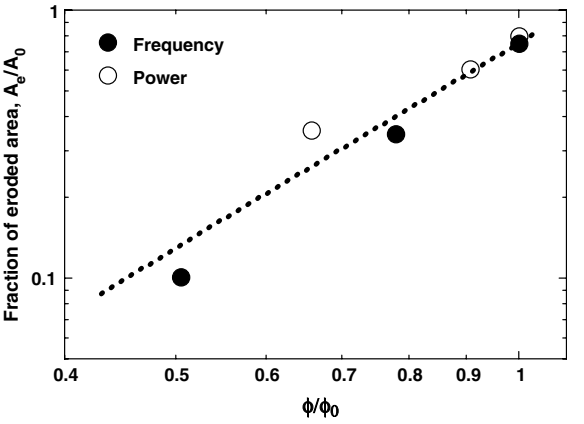

Fig. 16. Relationship between eroded fraction and ϕ/ϕ_0.

4. Discussion

In order to understand the cycle frequency effect on pitting damage formation, the bubble dynamics analysis was carried out using the following equation derived by Plesset [15]:

$$R\ddot{R}+\frac{3}{2}\dot{R}^2=\frac{1}{\rho}\left[\left(P_0+\frac{2\sigma}{R_0}-P_{\mathrm{V}}\right)\left(\frac{R_0}{R}\right)^{3\gamma}+P_{\mathrm{V}}-\frac{2\sigma}{R}-\frac{4\eta\dot{R}}{R}-P(t)\right], \tag{4}$$

$$P(t)=P_0+P_m\sin(\omega t). \tag{5}$$

Here, variables in Eqs. (4) and (5) are defined as shown in Fig. 17. The properties of mercury at 300 K were used for the simulation using Eq. (4). Fig. 18 illustrates the time response of bubble radius under the imposed impact with $P_m = 1$ MPa and period $T_0 = \omega/2\pi = 2$ ms. The bubble expands to approximately 2×10^4 times and varnishes around 14 ms. Fig. 19 shows the relationship between the life time of bubble and the period of imposed impact pressure, T_0. T_0 in the MIMTM is estimated to be approximately 2 ms. The imposed pressure

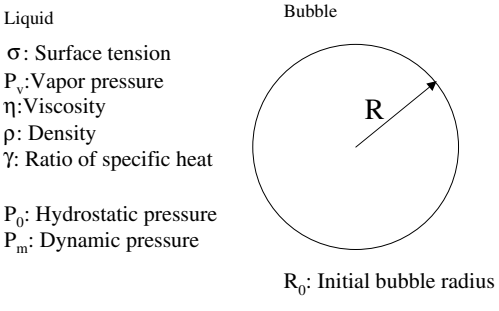

Fig. 17. Bubble dynamics simulation.

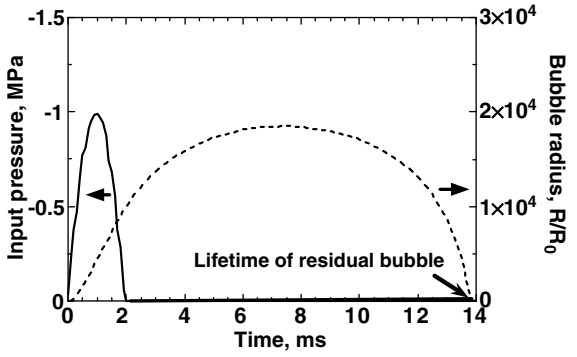

Fig. 18. Dynamic response of bubble.

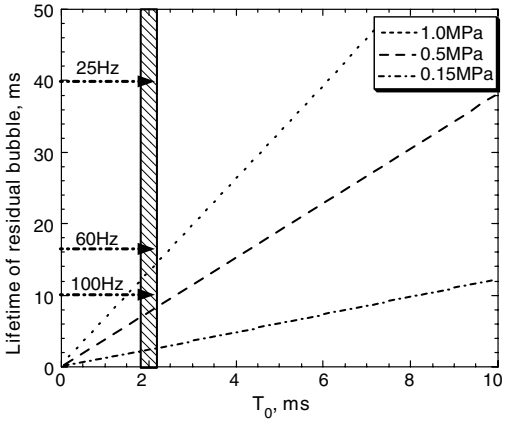

Fig. 19. Relationship between lifetime and impact duration in bubble.

around bubbles is unknown. P_m is varied from 0.15 MPa to 1.0 MPa. It is understandable from Fig. 19 that the possibility that the bubbles remain between repeated impacts is much higher in the cases of 100 Hz and 60 Hz than in 25 Hz. As a result, the residual bubbles might act as a damper at 60 Hz or 100 Hz against the localized impact due to cavity collapse. The pitting damage might be suppressed by the damping effect of residual bubbles, as compared with that at 25 Hz.

The incubation period is dependent on the power or pressure of imposed impact. As shown in Fig. 11, the incubation period might be defined as the number of cycles with the fraction of eroded area less than 1. In order to systematically and quantitatively evaluate the incubation period, we focused on the locus of fraction F against the number of cycles N. We carried out a numerical simulation on the locus using random function analysis [16] and derived the following equation:

$$F = 1 - \exp(CN). \quad (6)$$

Here, C is dependent on material and power or pressure. This equation is similar to the empirical one used to describe the coverage of shot peening [17]. Fig. 20 shows the fractions of various materials and impact conditions. The loci of fractions are adequately represented using Eq. (6). Hereafter, the incubation period is systematically defined as the period at $F = 0.98$. Fig. 21 shows the relationship between the power and the number of cycles in the incubation period estimated using Eq. (6). It is clearly understandable that the number of incubation cycles is dependent on the power applied to the mercury and the power threshold against the damage is unambiguously present. The incubation period is

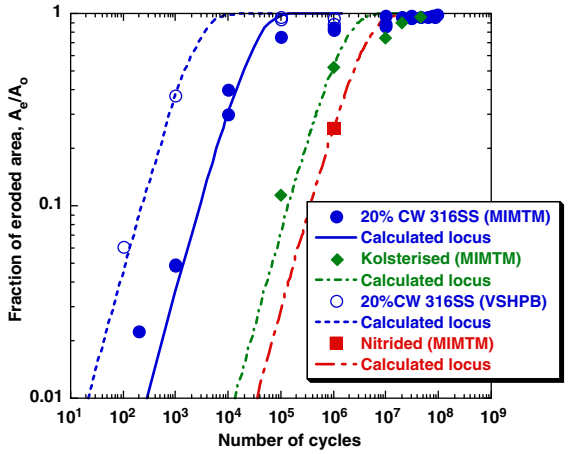

Fig. 20. Relationship between fraction of eroded area and number of cycles for 20% CW 316SS and several surface treatments.

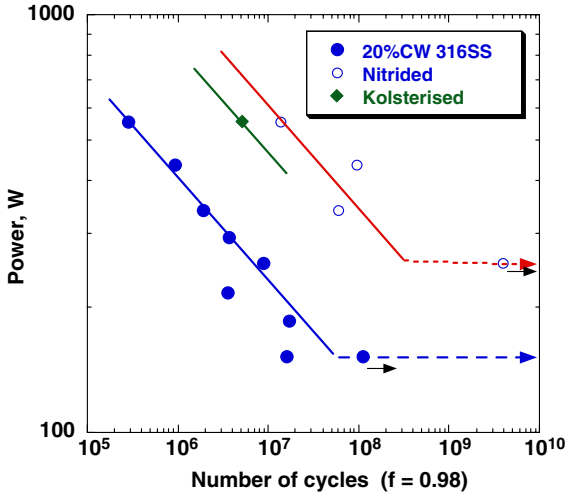

Fig. 21. Relationship between power and number of pulse cycles in the incubation period in MIMTM test.

prolonged by surface hardening treatment such as Kolsterising and nitriding.

Fig. 22 shows the normalized power, the MDE and the number of cycles, including data obtained by the WNR on-beam test. The power was normalized to 560 W in the MIMTM and to 1.2 MW in the WNR, because the morphology of the pitting damage at 560 W in the MIMTM is equivalent to that at 1.2 MW in the WNR. It is found from Fig. 22 that except for the 0.4 MW, the trend of the number of pulses in the incubation periods, N_i is described by the following equation:

$$\mathrm{Log}N_i = D - E\,\mathrm{Log\ Power}. \quad (7)$$

Here, D and E are constants in terms of materials and environment. It was suggested from Fig. 22 that $E = 3.8$ in the case of 20% CW 316SS. If the incubation cycles of pulses for a given power is known from Eq. (7), the MDE for any given number of pulses might be estimated using Eq. (1). That is, the formation of pitting damage is predictable by using Eqs. (1) and (7). Given a relationship between the MDE and the residual strength, RS, of damaged materials, the lifetime of the target associated with the pitting damage might be predicted based on the diagram illustrated in Fig. 23. It is, therefore, important to investigate the role of residual strength of pitting-damaged materials, in particular from the viewpoint of fatigue strength including mercury environment and irradiation damage, etc., because the target vessel will be bombarded repeatedly by impulsive pressure at some tens of Hz throughout its lifetime. For meaningful application of the erosion evaluation concept shown in Fig. 23 to the mercury target of a spallation source, more detailed relationships between simulation and on-beam tests must be established because a pressure generating mechanism is different

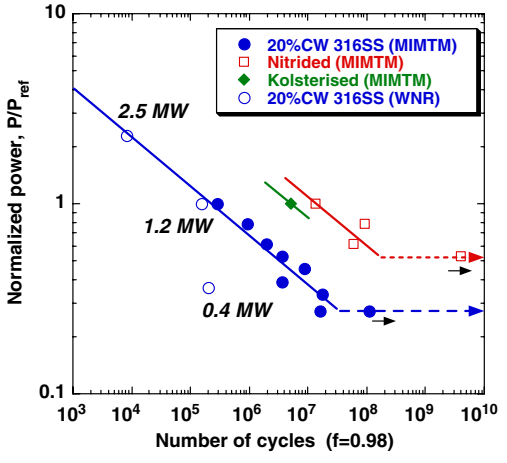

Fig. 22. Relationship between normalized power and number of pulse cycles in the incubation period.

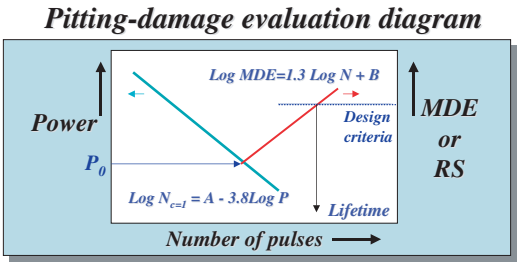

Incubation period is dependent on the materials and imposed power.

$\mathrm{Log}\ N_{c=1} = A - 3.8\mathrm{Log}\ P$

Nc=1:Number of pulses to end of incubation period

A : Material constant, Repeated frequency, etc.

After the eroded area fraction becomes nearly 100%, accelerated mass loss may start.

Mass loss MDE will be able to describe as follows

$\mathrm{Log\ MDE} = 1.3\ \mathrm{Log}\ N + B$

N: Number of pulses, B: f(material, power, etc.)

What is relationship between MDE and RS ?

The residual strength with pitting damage has to be evaluated from the viewpoint of fatigue and environment effects (mercury and irradiation, etc.)

Fig. 23. Concept of cavitation erosion evaluation in a mercury target.

between them. Additionally, a heat removal efficiency at the vessel/mercury may be affected by a void fraction due to generated cavities in mercury.

5. Conclusion

To simulate the pitting damage, that will be caused by a pulsed proton beam impinging on a mercury target, pressure pulse tests were performed using the MIMTM, which gives quite similar morphology of the pitting damage to that observed in WNR proton beam tests. The MDEs due to pitting damage obtained in the MIMTM were compared with classical vibratory horn tests and the estimated lifetime of a target involving pitting damage was discussed based on an analysis of bubble dynamics. The results are summarized as follows:

1. The pitting damage formation up to 10 million pulses is divided into 3 phases: In phase 1, isolated individual pits are formed up to 10^4 cycles; in phase 2, pits are combined and overlapped and the fraction of eroded area gets to be nearly 1 between 10^5 and 10^6 cycles; in phase 3, homogeneous erosion with accelerated mass loss starts between 10^6 and 10^7 cycles, in the case of 20% CW 3166SS in MIMTM.
2. The pitting damage can be characterized in two steps, an incubation period and a steady state erosion. During the steady state stage, mass loss scales with the number of cycles to approximately the 1.27 power for mercury.
3. The length of the incubation period is primarily a function of the material and the intensity of the power or pressure. There is a power threshold for the onset of pitting damage. A semi-empirical

equation was derived as a function of given power to estimate the incubation period.
4. The results of conclusion 2 and 3 provide a simple concept for evaluating the pitting damage against various materials and beam power.
5. The damage potential defined by high-frequency acceleration signals related with the localized impact by cavity collapse is useful to predict the pitting damage and might be applicable for a diagnostic monitoring system in the target.

Acknowledgments

The authors would like to thank Emeritus Professor N. Watanabe of JAERI for his fruitful advices and encouragement to this research work, Dr J.R. Haines and Mr B. Riemer of ORNL for supplying specimens, Mr Suzuki of JAERI for polishing specimens, Dr Kurata of JAERI for SEM observation, and Messrs T. Koyama and J. Yamamoto students at Ibaraki University for experimental assistance.

References

[1] Planning Division for Neutron Science, in: Proceeding of the 3rd Workshop on Neutron Science Project – Science and Technology in the 21st Century Opened by Intense Spallation Neutron Source, JAERI-Conf. 99-003, 1999.
[2] M. Futakawa, K. Kikuchi, H. Conrad, H. Stechemesser, Nucl. Instrum. and Meth. A 439 (2000) 1.
[3] M. Futakawa, H. Kogawa, R. Hino, J. Phys. IV France 10 (Pr9) (2000) 237.
[4] M. Futakawa, H. Kogawa, R. Midorikawa, R. Hino, H. Date, H. Takeishi, in: Proceedings of the 4th Int. Symp. Imp. Eng., 2001, p. 339.
[5] M. Futakawa, H. Kogawa, R. Hino, H. Date, H. Takeishi, Int. J. Impact Eng. 28 (2) (2003) 123.
[6] B. Riemer et al., Int. Workshop, Spal. Mats. Tech.-5, Charleston, South Carolina, 2002.
[7] M. Futakawa, H. Kogawa, C.C. Tsai, S. Ishikura, Y. Ikeda, JAERI-Research 2003-005, 2003.
[8] T. Bell, C.X. Li, Adv. Mater. Process. (June) (2002) 49.
[9] M.D. Kass, J.H. Whealton, N.E. Clapp Jr., J.R. DiStefano, J.H. DeVan, J.R. Haines, M.A. Akerman, T.A. Gabriel, Tribol. Lett. 5 (1998) 231.
[10] S.G. Young, J.R. Johnston, ASTM STP 408 (1967) 186.
[11] R. Garcia, F.G. Hammitt, R.E. Nystron, ASTM STP 408, Am. Soc. Testing Mats., 1967, p. 239.
[12] S. Pawel, E. Manneschmidt, Int. Workshop, Spal. Mats. Tech.-5, Charleston, South Carolina, USA, 2002.
[13] H. Soyama, M. Futakawa, Tribol. Lett. 17 (2004) 27.
[14] J. Haines, Cavitation Experts Meeting, October 2002.
[15] M.S. Plesset, J. Appl. Mech. 16 (1949) 277.
[16] H. Soyama, M. Futakawa, Numerical simulation of coverage of cavitation impacts changing with time, nihonkikaigakkai shukikoen-kai, 2003.
[17] SAE J443, 1984.